IEEE Access
Multidisciplinary | Rapid Review | Open Access Journal

Received April 20, 2020, accepted May 10, 2020, date of publication May 14, 2020, date of current version May 28, 2020.

Digital Object Identifier 10.1109/ACCESS.2020.2994830

Indirect Adaptive State-Feedback Control of Rotary Inverted Pendulum Using Self-Mutating Hyperbolic-Functions for Online Cost Variation

OMER SALEEM[1] AND KHALID MAHMOOD-UL-HASAN[2]
[1]Department of Electrical Engineering, National University of Computer and Emerging Sciences, Lahore 54000, Pakistan
[2]Department of Electrical Engineering, University of Engineering and Technology, Lahore 54000, Pakistan

Corresponding author: Omer Saleem (omer.saleem@nu.edu.pk)

ABSTRACT This paper presents the development of an indirect adaptive state-feedback controller to improve the disturbance-rejection capability of under-actuated multivariable systems. The ubiquitous Linear-Quadratic-Regulator (LQR) is employed as the baseline state-feedback controller. Despite its optimality, the LQR lacks robustness against parametric uncertainties. Hence, the main contribution of this paper is to devise and retrofit the LQR with a stable online gain-adjustment mechanism that dynamically adjusts the state weighting-coefficients of LQR's quadratic cost-function via state-error dependent nonlinear-scaling functions. An original self-mutating phase-based adaptive modulation scheme is systematically formulated in this paper to self-adjust the state weighting-coefficients. The scheme employs pre-calibrated secant-hyperbolic-functions whose waveforms are dynamically reconfigured online based on the variations in magnitude and polarity of state-error variables. This augmentation dynamically alters the solution of the Riccati-Equation which modifies the state-feedback gains online. The proposed adaptation flexibly manipulates the system's control effort as the response converges to or diverges from the reference. The efficacy of proposed adaptive controller is validated by conducting hardware-in-the-loop experiments to vertically stabilize the QNET 2.0 Rotary Pendulum system. As compared to the standard LQR, the proposed adaptive controller renders rapid transits in system's response with improved damping against oscillations, while maintaining its asymptotic-stability, under bounded exogenous disturbances.

INDEX TERMS Hyperbolic functions, linear quadratic regulator, cost-function, rotary inverted pendulum, self-tuning control, state weighting-coefficients.

I. INTRODUCTION

The adaptive systems are used to efficiently compensate the rapid dynamic variations in the plant by autonomously modifying the controller's characteristics [1]. Hence, they are immensely favored for controlling multivariable under-actuated systems, such as, self-balancing robots, rotor-crafts, and robotic manipulators, etc [2], [3]. The rotary inverted pendulum is a nonlinear and open-loop unstable system that is widely used as a benchmark to analyze the efficacy of control algorithms for under-actuated systems [4].

A plethora of feedback controllers have been designed to optimally stabilize the self-erecting pendulums [5]. The proportional-integral-derivative (PID) controllers are widely favored due to their simple structure and reliable yield [6]. However, the linear weighted sum of error variables limits their performance under abrupt parametric variations [7]. The fractional-order controllers are generally preferred due to their capability of realizing the system's un-modeled nonlinearities [8]. However, the offline selection of fractional orders is an ill-posed problem. The fuzzy controllers, despite their flexibility, require elaborate qualitative logical rules and offline tuning of a multitude of parameters to deliver robust control effort [9]. The sliding mode controllers, despite their robustness, unavoidably inject chattering in the system's response [10], [11]. The ubiquitous Linear-Quadratic-Regulator (LQR) is a state-feedback controller that yields stable and optimal control decisions by minimizing a quadratic performance criterion that captures the state and control-input variations [12]. However, owing

The associate editor coordinating the review of this manuscript and approving it for publication was Guolong Cui.

to its dependence on state-space model, the LQR's performance gets severely degraded under the influence of model variations and identification errors [13].

The performance limitations associated with the conventional controllers for rotary pendulums can be rectified by augmenting the baseline feedback controller with an online adaptation law that dynamically alters the controller's characteristics in real-time [14]. Such adaptive mechanisms enhance the system's response speed, damping strength, and resilience against exogenous disturbances [15]. These attributes help in achieving good position-regulation accuracy, across a broad range of conditions, which is normally unattainable via linear compensators [16], [17]. The model-reference-adaptive-system minimizes the error between the outputs of the actual system and a reference model in order to modify the critical control parameters [18]. However, accurate identification of the reference model is a difficult task due to the complex dynamics of higher-order systems [19].

In self-tuning systems, generally a set of pre-defined analytical (or logical) rules are adopted to vary the controller-parameters [20]. The gain-scheduling mechanism employs pre-defined switching rules to commute between specifically designed linear controllers under different operating conditions [21]. However, the individual calibration of a large number of linear controllers that offer good control performance and asymptotic-stability is a cumbersome task. The linear-parameter-varying (LPV) technique is an automatic gain-scheduler that dynamically changes the parameters of system's state-space model as a function(s) of state-variables [22]. Despite the robustness and stability of this technique, it is difficult to derive accurate LPV models for nonlinear systems owing to their complex dynamics [23]. The State-Dependent-Riccati-Equation based control strategies are widely favored to control the inherently unstable systems with nonlinear dynamics [24]. However, it is quite hard to accurately define the state-dependent coefficient matrices that fully realize the system's nonlinear characteristics. The technique involving online dynamic adjustment of weighting-factors of the optimal controller's cost-function, to indirectly self-tune the state-feedback gains, has garnered a lot of attention recently [25].

The augmentation of nonlinear scaling functions with linear compensators to self-adjust critical gains is extensively used in controlling non-minimum phase systems [26], [27]. The nonlinear-type state-feedback controllers significantly improve the system's response speed, damping against disturbances, tracking accuracy, and control input economy [28]–[30]. There are two main categories of nonlinear-scaling functions that are widely used. The most commonly used category involves adaptive parameter adjustment using only the magnitude of the state-error variables [14]. The second category involves the online parameter adjustment based on the magnitude as well as the direction-of-variation (or phase) of the state-error [31]. The inclusion of phase information in the modulation scheme improves the adaptability of controller as the response deviates from or converges towards the reference [32].

The **main contribution** of this paper is to devise an original indirect phase-driven self-tuning controller for an under-actuated rotary inverted pendulum system. The proposed work aims at improving the system's damping against fluctuations and response speed, while preserving its stability across the entire operating regime. The indirect dynamic adjustment of the state-feedback gains is done by adaptively modulating the state weighting-coefficients associated with the controller's quadratic cost-function. The updated coefficients modify the solution of Riccati Equation, and hence the state-feedback gains, after every sampling interval. The nonlinear scaling of state weighting-coefficients is initiated by using a conventional paradigm that employs pre-calibrated set of Secant-Hyperbolic-Functions (SHFs) to manipulate the weights according to the movement of system's time-domain response [33]. However, to further enhance the controller's adaptability and resilience, the aforementioned paradigm is methodically evolved by formulating a unique self-mutating structure of SHFs to adaptively modulate the coefficients. The proposed adaptation law uses real-time measurements of magnitude and polarity of state-error variables to automatically mutate a growing SHF into a decaying SHF, and vice-versa. The self-mutating SHF arrangement offers efficient and smooth transition of state-feedback gains across a wide range of operating conditions. It strengthens the controller's damping against overshoots and reduces transient-recovery time under exogenous disturbances. The benefits afforded by the proposed adaptive controller are verified via credible hardware-in-the-loop experiments conducted on the QNET 2.0 Rotary Pendulum (Rot-Pend) board [14].

The idea of adaptively tuning the state weighting-coefficients via the proposed original ''self-mutating SHFs'', to enhance the robustness of self-tuning LQR for under-actuated systems, has not been attempted previously in the available open literature. Hence, this paper mainly focuses on the realization of this novel idea.

The remaining paper is organized as follows. The mathematical model of the Rot-Pend is presented in Section 2. The theoretical background of LQR is discussed in Section 3. The design of proposed adaptive control procedure is presented in Section 4. The self-mutating weight adjustment scheme is formulated in Section 5. The details regarding the experimental analysis are presented in Section 6. The article is concluded in Section 7.

II. MATHEMATICAL MODEL

The Rot-Pend is an inherently unstable system with highly nonlinear dynamics, which make it an ideal candidate to examine and validate the robustness of the proposed phase-driven adaptive control system [34]. The hardware schema of the Rot-Pend setup is shown in Figure 1. The yaw motion of pendulum's arm is denoted as α.

The arm rotates about the z-axis via a permanent magnet DC motor, which provides the required energy to swing-up

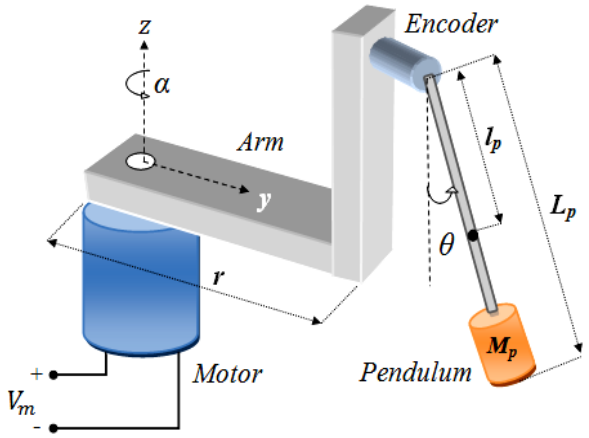

FIGURE 1. Simplified schematic of a rotary inverted pendulum.

the pendulum's rod. The angular displacement of the rod is referred to as θ. The state-space representation of a linear dynamical system is given by (1) and (2).

$$\dot{x}(t) = \boldsymbol{A}x(t) + \boldsymbol{B}u(t) \tag{1}$$
$$y(t) = \boldsymbol{C}x(t) + \boldsymbol{D}u(t) \tag{2}$$

where, x is the state-vector, y is the output-vector, u is the control input signal, $\boldsymbol{A}$ is the state-transition matrix, $\boldsymbol{B}$ is the input matrix, $\boldsymbol{C}$ is the output matrix, and $\boldsymbol{D}$ is the feed-forward matrix. The state-vector and the control input-vector of the Rot-Pend system are identified in (3) and (4), [34].

$$x(t) = \begin{bmatrix} \alpha(t) & \theta(t) & \dot{\alpha}(t) & \dot{\theta}(t) \end{bmatrix}^T \tag{3}$$
$$u(t) = V_m \tag{4}$$

where, V_m is voltage signal applied to control the DC motor. The nominal state-space model of the Rot-Pend system is defined in (5), [14].

$$A = \begin{bmatrix} 0 & 0 & 1 & 0 \\ 0 & 0 & 0 & 1 \\ 0 & a_1 & a_2 & 0 \\ 0 & a_3 & a_4 & 0 \end{bmatrix}, \quad B = \begin{bmatrix} 0 \\ 0 \\ b_1 \\ b_2 \end{bmatrix},$$
$$C = \begin{bmatrix} 1 & 0 & 0 & 0 \\ 0 & 1 & 0 & 0 \\ 0 & 0 & 1 & 0 \\ 0 & 0 & 0 & 1 \end{bmatrix}, \quad D = \begin{bmatrix} 0 \\ 0 \\ 0 \\ 0 \end{bmatrix} \tag{5}$$

where,

$$a_1 = \frac{rM_p^2 l_p^2 g}{J_p J_e + J_e l_p^2 M_p + J_p M_p r^2},$$
$$a_2 = \frac{-K_t K_m \left(J_p + M_p l_p^2\right)}{\left(J_p J_e + J_e l_p^2 M_p + J_p M_p r^2\right) R_m},$$
$$a_3 = \frac{M_p l_p g \left(J_e + M_p r^2\right)}{J_p J_e + J_e l_p^2 M_p + J_p M_p r^2},$$
$$a_4 = \frac{-r M_p l_p K_t K_m}{\left(J_p J_e + J_e l_p^2 M_p + J_p M_p r^2\right) R_m},$$
$$b_1 = \frac{K_t \left(J_p + M_p l_p^2\right)}{\left(J_p J_e + J_e l_p^2 M_p + J_p M_p r^2\right) R_m},$$
$$b_2 = \frac{r M_p l_p K_t}{\left(J_p J_e + J_e l_p^2 M_p + J_p M_p r^2\right) R_m}$$

The system's model parameters are clearly described and their values are identified in Table 1 [14].

TABLE 1. Model parameters of QNET 2.0 rotary pendulum system.

Parameter symbol	Parameter description	Identified value
M_p	Mass of pendulum	0.027 kg
l_p	Pendulum center of mass	0.153 m
L_p	Length of pendulum rod	0.191 m
r	Length of horizontal arm	0.083 m
M_{arm}	Mass of arm	0.028 kg
g	Gravitational acceleration	9.810 m/s^2
J_e	Moment about motor shaft	1.23×10^{-4} kgm^2
J_p	Moment about pendulum	1.10×10^{-4} kgm^2
R_m	Motor armature resistance	3.30 Ω
L_m	Motor armature inductance	47.0 mH
K_t	Motor torque constant	0.028 N.m
K_m	Back e.m.f. constant	0.028 V/(rad/s)
T_m	Maximum torque	0.14 Nm

III. PRIMARY STATE-FEEDBACK CONTROLLER

The LQR is a state-feedback controller that has gained a lot of traction in the field of multivariable control systems [35].

It delivers optimal control decisions by minimizing a quadratic cost-function that captures the variations in state-variables and control-input associated with the linear multivariable system. The quadratic cost-function is shown in (6), [36].

$$J_{lq} = \frac{1}{2}\int_0^\infty \left[x(t)^T \boldsymbol{Q}x(t) + u(t)^T \boldsymbol{R}u(t)\right] dt \tag{6}$$

where, $\boldsymbol{Q} \in \mathbb{R}^{4\times4}$ and $\boldsymbol{R} \in \mathbb{R}$ are the state and control weighting-matrices, respectively. The state and control-weighting matrices are selected such that $\boldsymbol{Q} = \boldsymbol{Q^T} \geq 0$ and $\boldsymbol{R} > 0$, respectively. For the given system, these matrices are symbolically represented as shown in (7).

$$\boldsymbol{Q} = diag\begin{pmatrix} q_\alpha & q_\theta & q_{\dot{\alpha}} & q_{\dot{\theta}} \end{pmatrix}, \quad \boldsymbol{R} = m \tag{7}$$

where, q_x and m are the real-numbered positive state and control weighting-coefficients of these matrices, respectively. The state weighting-coefficients are heuristically selected by iteratively minimizing the cost-function J_e, shown in (8), to attain the best position-regulation accuacy.

$$J_e = \int_0^\infty |e_\alpha(t)|^2 + |e_\theta(t)|^2 + |u(t)|^2 \, dt$$
$$\text{such that, } e_\theta(t) = \pi - \theta(t), \quad e_\alpha(t) = \alpha_{ref} - \alpha(t) \tag{8}$$

The initial angular displacement of pendulum's arm is chosen as its reference position, α_{ref}, for every experimental trial. A small value of m renders peak servo requirements which often leads to actuator saturation. Whereas, a larger value of m degrades the time-optimality of pendulum's angular response while attempting to minimize the control energy expenditure. Hence, in this research, the value of m is fixed at unity. The selected coefficients of $\boldsymbol{Q}$ and $\boldsymbol{R}$ matrices are shown in (9).

$$\boldsymbol{Q} = diag\begin{pmatrix} 32.8 & 52.2 & 6.1 & 2.5 \end{pmatrix}, \quad \boldsymbol{R} = 1 \tag{9}$$

The selected coefficients are used to compute the solution, $\boldsymbol{P}$, of the Algebraic Riccati Equation (ARE) shown in (10).

$$\boldsymbol{A}^T\boldsymbol{P} + \boldsymbol{P}\boldsymbol{A} - \boldsymbol{P}\boldsymbol{B}\boldsymbol{R}^{-1}\boldsymbol{B}^T\boldsymbol{P} + \boldsymbol{Q} = 0 \tag{10}$$

where, $\boldsymbol{P} \in \mathbb{R}^{4\times4}$ is a symmetric positive-definite matrix. The solution of ARE guarantees an asymptotically-convergent control behavior if the system is controllable. This is a sufficient proof of stability for the LQ control systems. Finally, the matrix $\boldsymbol{P}$ is used to calculate the Kalman gain vector, $\boldsymbol{K}$, as shown below.

$$\boldsymbol{K} = \boldsymbol{R}^{-1}\boldsymbol{B}^T\boldsymbol{P} \tag{11}$$

The fixed Kalman gain vector calculated offline in this research is $\boldsymbol{K} = \begin{bmatrix} -6.18 & 137.42 & -4.42 & 18.81 \end{bmatrix}$. The linear control law in (11) is also retrofitted with additional control terms associated with the integral-of-error in α and θ, in order to damp the angular fluctuations while tracking the reference [37]. The consolidated integral controller is expressed in (12)

$$u_I(t) = \boldsymbol{K}_I\varepsilon(t) = \begin{bmatrix} K_{I\alpha} & K_{I\theta} \end{bmatrix}\begin{bmatrix} \varepsilon_\alpha(t) \\ \varepsilon_\theta(t) \end{bmatrix}$$
$$\text{such that, } \varepsilon_\alpha(t) = \int_0^t e_\alpha(\tau)d\tau, \ \varepsilon_\theta(t) = \int_0^t e_\theta(\tau)d\tau \tag{12}$$

The integral gains are tuned via trial-and-error by iteratively minimizing the cost-function J_e, shown in (8), to obtain optimum position-regulation behavior. The selected integral gains are given by $\boldsymbol{K}_I = \begin{bmatrix} -2.06 & -7.47\times10^{-6} \end{bmatrix}$. The linear control law is given by (13).

$$u(t) = -\boldsymbol{K}x(t) + \boldsymbol{K}_I\varepsilon(t) \tag{13}$$

IV. PROPOSED ADAPTIVE CONTROLLER DESIGN

In order to synthesize a stable self-tuning LQR, the state-feedback gains are dynamically adjusted after every sampling interval by using an indirect hierarchical adaptive modulation scheme. Where in, the coefficients of state-penalty matrix, q_x, are modified online using phase-driven nonlinear scaling functions [25]. This arrangement obviates the requirement of empirically tuning the q_x under different operating conditions. The pre-calibrated nonlinear scaling functions utilize the real-time measurements of the state-error variables to adaptively modulate the values of q_x. The resulting time-varying state weighting-matrix, $\boldsymbol{Q}(t)$, is shown in (14).

$$\boldsymbol{Q}(t) = diag\begin{pmatrix} q_\alpha(t) & q_\theta(t) & q_{\dot\alpha}(t) & q_{\dot\theta}(t) \end{pmatrix} \tag{14}$$

The value of ρ is fixed at unity to regulate the control input expenditure and position-regulation accuracy under every operating condition. The corresponding Riccati Equation is shown in (15), [24], [36].

$$\boldsymbol{A}^T\boldsymbol{P}(t) + \boldsymbol{P}(t)\boldsymbol{A} - \boldsymbol{P}(t)\boldsymbol{B}\boldsymbol{R}^{-1}\boldsymbol{B}^T\boldsymbol{P}(t) + \boldsymbol{Q}(t) = -\dot{P}(t) \tag{15}$$

In an infinite-horizon control problem, the derivative-term $\dot{\boldsymbol{P}}(t)$ converges to zero [36]. Hence, the Riccati Differential Equation is simplified to Matrix Riccati Equation as follows.

$$\boldsymbol{A}^T\boldsymbol{P}(t) + \boldsymbol{P}(t)\boldsymbol{A} - \boldsymbol{P}(t)\boldsymbol{B}\boldsymbol{R}^{-1}\boldsymbol{B}^T\boldsymbol{P}(t) + \boldsymbol{Q}(t) = 0 \tag{16}$$

The solution, $\hat{\boldsymbol{P}}(t)$, of the aforementioned Riccati Equation is automatically updated after every sampling interval. This arrangement modifies the Kalman gains. The expression for time-varying Kalman gain vector is given in (17).

$$\boldsymbol{K}(t) = \boldsymbol{R}^{-1}\boldsymbol{B}^T\boldsymbol{P}(t) \tag{17}$$

The proposed Self-Tuning-Regulator (STR) is defined as follows.

$$\hat{u}(t) = -\boldsymbol{K}(t)x(t) + \boldsymbol{K}_I\varepsilon(t) \tag{18}$$

The integral gains in $\boldsymbol{K}_I$ are maintained at their original (prescribed) values. The proposed adaptive control system is shown in Figure 2. This scheme avoids the learning burden of extended state-observers used in conventional active disturbance-rejection controllers for uncertain systems [26].

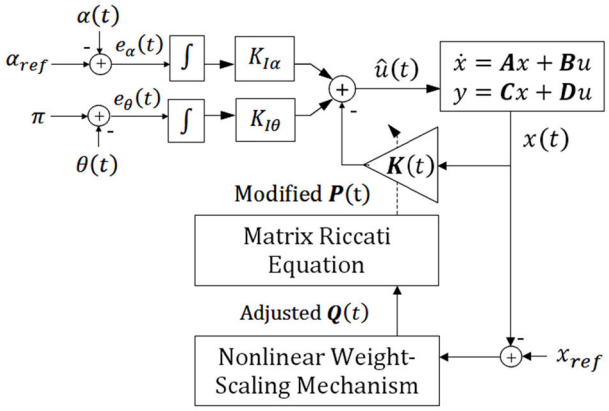

FIGURE 2. Block diagram of proposed adaptive control framework.

The stability proof for the proposed adaptive controller is obtained by considering the following Lyapunov function.

$$V(t) = x(t)^T\boldsymbol{P}(t)x(t) > 0, \quad \text{for } x(t) \neq 0 \tag{19}$$

The time-derivative of $V(t)$ must be negative-definite for the system to be asymptotically-stable [36]. The expression of the first-derivative of $V(t)$ is provided as follows [36].

$$\dot{\boldsymbol{V}}(t) = x(t)^T\Big(\dot{\boldsymbol{P}}(t) + \boldsymbol{A}^T\boldsymbol{P}(t) + \boldsymbol{P}(t)\boldsymbol{A} - \boldsymbol{P}(t)\boldsymbol{B}\boldsymbol{R}^{-1}\boldsymbol{B}^T\boldsymbol{P}(t)\Big)x(t) \tag{20}$$

By substituting the matrix Riccati Equation, given in (15), in the above expression, the $\dot{V}(t)$ is simplified as follows.

$$\dot{V}(t) = -\left(x(t)^T \boldsymbol{Q}(t)\, x(t)\right) < 0 \tag{21}$$

The expression shows that $\dot{V}(t) < 0$ if $\boldsymbol{Q}(t) > 0$ and thus, guarantees stability.

V. NONLINEAR WEIGHT-SCALING MECHANISM

As discussed earlier, a nonlinear-type self-tuning mechanism is employed in this research to adaptively modulate the coefficients of $\boldsymbol{Q}(t)$. The proposed adaptation enhances the controller's immunity against modeling uncertainties, transient load changes, lumped disturbances, process noise, and actuator limitations, etc. Two different nonlinear-type adaptive weight-scaling mechanisms are synthesized in the following sub-sections by employing Secant-Hyperbolic-Functions (SHFs). The SHFs are utilized owing to their symmetry, bounded nature, and smoothness [18], [30]. The proposed adaptation mechanism is simply based on a set of algebraic equations that does not entail recursive computational burden on the embedded processor.

A. BASELINE PHASE-BASED FUNCTIONS

This scheme employs SHFs as the baseline adapter functions. The shapes of SHF waveforms are altered in accordance with the "phase" of response. These phase-driven functions contain the complete information of the magnitude and polarity of state-error variables, which makes them highly effective for damping control applications. The proposed scheme is constituted in accordance with the following qualitative rules [32], [33].

1. The proportional weights, q_α and q_θ, are maintained at a constant value as long as the angular-response stays within a narrow (predefined) bandwidth of the reference value. This hysteresis-type controller prevents limit-cycles caused by system's static friction at very low error conditions [38]. Beyond this dead zone, the proportional weights are inflated as the error-magnitude increases in order to strengthen the damping effort.
2. The differential weights, $q_{\dot{\alpha}}$ and $q_{\dot{\theta}}$, are inflated when error and error-derivative have same polarities. This phenomenon implies that the response is diverging from the reference, which incites the application of a relatively stiffer control effort to damp the overshoots (or undershoots) and reverse the direction of response. Conversely, the differential weights are depressed when error and error-derivative have opposite polarities, which implies that the response is moving towards the reference and thus, requires a softer control effort so the response can quickly settle with minimum fluctuations.

These qualitative rules are synthesized with the objective to further improve the system's error convergence-rate and damping strength. The formulation of the baseline phase-based SHFs is presented as follows.

$$\begin{aligned} q_\alpha(t) &= a_\alpha - b_\alpha.[\operatorname{sech}(\gamma_\alpha.e_\alpha(t) + \beta_\alpha) \\ &\quad + \operatorname{sech}(\gamma_\alpha.e_\alpha(t) - \beta_\alpha)] \end{aligned} \tag{22}$$

$$\begin{aligned} q_\theta(t) &= a_\theta - b_\theta.[\operatorname{sech}(\gamma_\theta.e_\theta(t) + \beta_\theta) \\ &\quad + \operatorname{sech}(\gamma_\theta.e_\theta(t) - \beta_\theta)] \end{aligned} \tag{23}$$

$$\begin{aligned} q_{\dot{\alpha}}(t) &= m_\alpha.(a_{\dot{\alpha}} - b_{\dot{\alpha}} \operatorname{sech}(\gamma_\alpha.e_\alpha(t))) \\ &\quad + \frac{a_{\dot{\alpha}} - b_{\dot{\alpha}}}{1 + |\sigma_\alpha.e_\alpha(t)|^2} \end{aligned} \tag{24}$$

$$\begin{aligned} q_{\dot{\theta}}(t) &= m_\theta.\left(a_{\dot{\theta}} - b_{\dot{\theta}} \operatorname{sech}(\gamma_\theta.e_\theta(t))\right) \\ &\quad + \frac{a_{\dot{\theta}} - b_{\dot{\theta}}}{1 + |\sigma_\theta.e_\theta(t)|^2} \end{aligned}$$

$$\begin{aligned} \text{such that, } m_\alpha &= \operatorname{step}(e_\alpha(t) \times \dot{e}_\alpha(t)), \\ m_\theta &= \operatorname{step}(e_\theta(t) \times \dot{e}_\theta(t)) \end{aligned} \tag{25}$$

where, a_x and b_x are the positive upper and lower bounds of each function such that $a_x \geq b_x$ to ensure $q_x(t) \geq 0$ always, 'x' denotes the state-variable being considered, γ_x represents the variation-rate of each function, sech (.) represents the SHF, and m_x is a step (.) function that yields a "zero" if its internal argument has a negative value and a "one" if its internal argument has a positive value. The parameters σ_α and σ_θ are the scaling-factors of the associated state-error variables. These hyper-parameters are tuned offline by minimizing J_e to yield strong damping control. The tuned parameters are shown in Table 2. The dead-zones of α and θ are experimentally identified as $\beta_\alpha = 0.20$ rad. and $\beta_\theta = 0.015$ rad., respectively.

TABLE 2. Tuned parameters of baseline hyperbolic functions.

Parameter symbol	Selection range	Tuned value
a_α	[0, 500]	351.60
b_α	[0, 500]	168.45
a_θ	[0, 500]	200.00
b_θ	[0, 500]	95.55
$a_{\dot{\alpha}}$	[0, 50]	10.15
$b_{\dot{\alpha}}$	[0, 50]	5.42
$a_{\dot{\theta}}$	[0, 50]	8.22
$b_{\dot{\theta}}$	[0, 50]	4.36
γ_α	[0, 50]	6.10
γ_θ	[0, 50]	19.88
σ_α	[0, 50]	2.11
σ_θ	[0, 50]	5.95

The m_x setting in $q_{\dot{\alpha}}(t)$ and $q_{\dot{\theta}}(t)$ activates the damping controller which enlarges the differential weights when the error and error-derivative have same polarities (divergence). The damping controller is de-activated when the error and error-derivative have opposite polarities (convergence).

The second nonlinear function used in $q_{\dot{\alpha}}(t)$ and $q_{\dot{\theta}}(t)$ is insignificant under large error conditions. However, as the response converges, it immediately switches the differential weights to a lower value and then gradually inflates them to speed up the transient recovery speed. The dynamically-adjusted values of $q_x(t)$ remain positive and bounded which

ensure the system's stability. The adaptive control system equipped with the aforementioned phase-based SHFs is denoted as the "Baseline-STR".

B. SELF-MUTATING PHASE-BASED FUNCTIONS

In this sub-section, the proposed phase-driven self-mutating SHF based modulation scheme is systematically formulated by utilizing the information of magnitude and phase of the state-error dynamics to adaptively tune the state weighting coefficients during real-time applications. The utilization of phase information in conjunction with the self-mutation capability, harnesses the ability of proposed adapters to efficiently compensate the abrupt parametric variations while regulating the position. The general expression of a self-mutating SHF is given in (26).

$$q_x(t) = m_x.a_x - (b_x - (1 - m_x).a_x).\text{sech}(\gamma_x.e_x(t)) \quad (26)$$

These SHFs are formulated by using similar qualitative rules as discussed in the previous sub-section.

1) SELF-MUTATION SCHEME

The weight-adjusting functions, $q_x(t)$, are augmented with the Boolean operators, m_α and m_θ, that automatically transform the decaying behaviour of the waveform into a growing behaviour as the response diverges from or converges towards the reference, and vice-versa. Consider the error profile of an arbitrary under-damped system shown in Figure 3. The error profile is divided in four phases; A, B, C, and D. Each phase represents a distinct operating condition that is addressed individually to attain best control effort. The logical rules governing the self-mutation of $q_x(t)$, shown in (26), with respect to the changes in the state of Boolean operator, m_x, are defined in Table 3. The self-mutation scheme is illustrated in Figure 4.

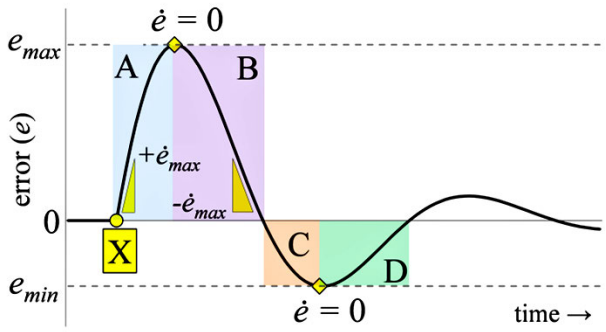

FIGURE 3. Error profile of a disturbed under-damped system.

TABLE 3. Logical rules for self-mutation of weight-adjusting functions.

m_x	Movement of response	Mutation of $q_x(t)$ waveform
1	Diverging from reference	$\bar{q}_x(t) = a_x - (b_x.\text{sech}(\gamma_x.e_x(t)))$
0	Converging to reference	$\acute{q}_x(t) = (a_x - b_x).\text{sech}(\gamma_x.e_x(t))$

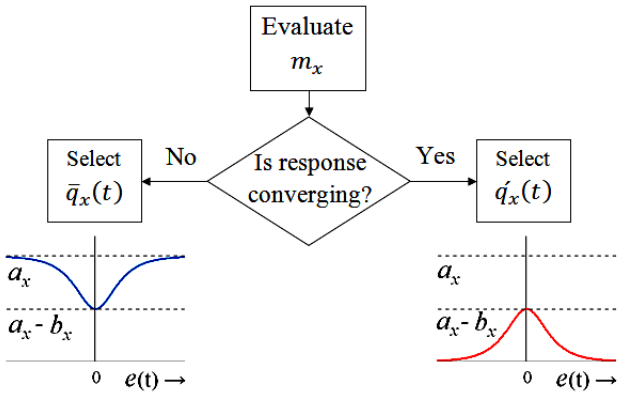

FIGURE 4. Self-mutation scheme for weight-adjusting functions.

The weight adjustment strategy governed by the proposed paradigm is as follows. When a disturbance is applied, the response moves away from reference as shown in phase-A of Figure 3. The corresponding Boolean-setting of $m_x = 1$ renders a growing function of the form, $\bar{q}_x(t)$, as shown in Table 3. Due to the increasing error magnitude in this phase, the weighting-coefficients initiate from $a_x - b_x$ and gradually rise to a_x, as the response reaches its peak (See Figure 4). This arrangement damps the overshoots and quickly changes the direction of response. As the response reverses its direction and starts moving towards the reference, as shown in phase-B of Figure 3, the Boolean-setting of $m_x = 0$ renders a decaying function of the form, $\acute{q}_x(t)$, as shown in Table 3. The coefficients immediately switch to a much smaller value, as shown in Figure 4, to soften the control effort. From this point onwards, the coefficients are gradually inflated towards $a_x - b_x$, which allows the response to settle quickly and smoothly. Upon reaching the reference, the response continues to propagate in the same direction due to the system's moment-of-inertia. This phenomenon leads to a negative error as shown in phase-C of Figure 3. Hence, the setting of $m_x = 1$ is automatically re-engaged which mutates the weighting-function back to $\bar{q}_x(t)$. When the response reverts back, as shown in phase-D, the weights are modulated according to $\acute{q}_x(t)$ once again. The variation pattern of $q_x(t)$, in every phase, is illustrated in Figure 5.

2) DAMPING MODULATOR

Each SHF is also augmented with a Damping-Modulator (DM) that is only activated under abrupt parametric variations when the state-error derivative of the response becomes considerably large [39]. Under such conditions, the DM measures the error-derivative magnitude and accordingly relocates the inflation-point, $a_x - b_x$, of $q_x(t)$. The DM functions are implemented as follows.

$$z_\alpha(t) = \rho_{min} + \frac{\rho_{max} - \rho_{min}}{1 + |\mu_\alpha.\dot{e}_\alpha(t)|^4} \quad (27)$$

$$z_\theta(t) = \rho_{min} + \frac{\rho_{max} - \rho_{min}}{1 + |\mu_\theta.\dot{e}_\theta(t)|^4} \quad (28)$$

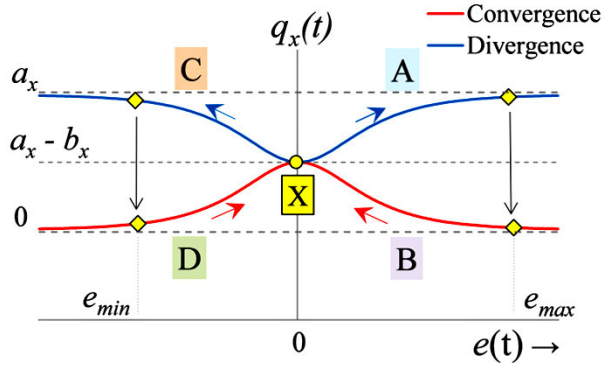

FIGURE 5. Variation rules for weighting coefficients in every phase.

TABLE 4. Tuned parameters of damping-modulator functions.

Parameter symbol	Selection range	Tuned value
ρ_{min}	[0.5, 1.0]	0.81
ρ_{max}	[1.0, 1.5]	1.02
μ_α	[0, 50]	2.93
μ_θ	[0, 50]	7.85

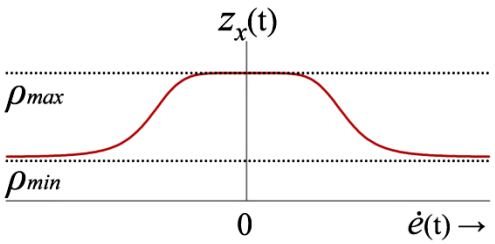

FIGURE 6. Waveform of the Damping-Modulator (DM) function.

where, ρ_{min} and ρ_{max} are the upper and lower bounds of the DM functions. Same set of bounds are used for $z_\alpha(t)$ and $z_\theta(t)$. The μ_α and μ_θ are positive real-numbered scaling constants that are empirically tuned by minimizing J_e to attain minimal oscillations in the response. Their selected values are shown in Table 4. The exponent of $\dot{e}_x(t)$ variable in DM functions is selected as four, so that $z_x(t)$ maintains its value at ρ_{max} for a broad bandwidth of error-derivatives and only varies when the magnitude of error-derivative is considerably large, as shown in Figure 6. The synthesized DM functions are implanted in $q_x(t)$, expressed in (26), as an adaptive scaling factor for the b_x constants.

With this augmentation, the SHFs reconfigure themselves under disturbances as depicted in Figure 7. The proposed self-mutating phase-based SHFs are formulated as follows.

$$q_\alpha(t) = m_\alpha.a_\alpha - (z_\alpha(t).b_\alpha - (1-m_\alpha).a_\alpha).\text{sech}(\gamma_\alpha.e_\alpha(t)) \quad (29)$$

$$q_\theta(t) = m_\theta.a_\theta - (z_\theta(t).b_\theta - (1-m_\theta).a_\theta).\text{sech}(\gamma_\theta.e_\theta(t)) \quad (30)$$

$$q_{\dot\alpha}(t) = m_\alpha.a_{\dot\alpha} - (z_\alpha(t).b_{\dot\alpha} - (1-m_\alpha).a_{\dot\alpha}).\text{sech}(\gamma_{\dot\alpha}.e_\alpha(t)) \quad (31)$$

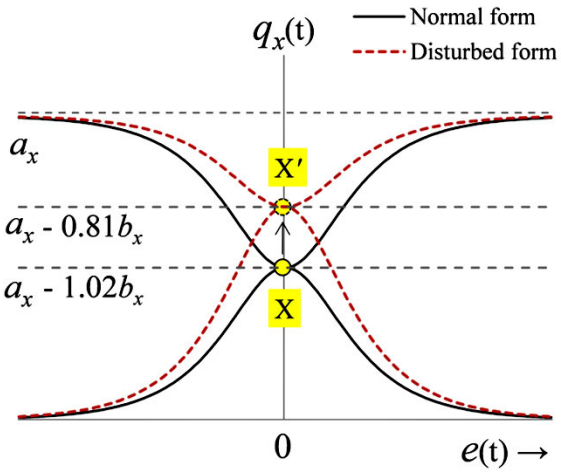

FIGURE 7. Reconfiguration of the SHF under disturbance.

$$q_{\dot\theta}(t) = m_\theta.a_{\dot\theta} - (z_\theta(t).b_{\dot\theta} - (1-m_\theta).a_{\dot\theta}).\text{sech}(\gamma_{\dot\theta}.e_\theta(t)) \quad (32)$$

The self-mutating SHFs utilize the same value of a_x, b_x, and γ_x as shown in Table 2. The adapted values of $q_x(t)$ remain positive throughout the operating regime, which ensures the system's stability. The controller equipped with the Self-Mutating SHFs is denoted as the "SM-STR".

VI. EXPERIMENTAL EVALUATION

This section presents the hardware setup details, the experimentation procedure, and the analysis of results.

A. EXPERIMENTAL SETUP

The QNET 2.0 Rotary Pendulum board, shown in Figure 8, is used to examine the proposed control schemes via hardware-in-the-loop experiments [14].

The real-time variations in α and θ are measured via rotary encoders that are commissioned at the pendulum's pivot and motor's shaft, respectively. The data samples are acquired at 1000 Hz by using the NI-ELVIS II data-acquisition board. The processed data is serially transported at 9600 bps to the control software that is running on a digital computer with 2.0 GHz processor and 6.0 GB RAM. The customized control application is implemented in a virtual instrument file of the LabVIEW software by using its Block Diagram tool. The mathematical objects are acquired from its functions palette. The SHFs are implemented by coding a C-language program in the Math-Script module. The flow chart of control algorithm is shown in Figure 9. The front-end panel of control application serves as a user-interface for the graphical visualization of state-variations.

The control signals are serially transmitted to a Pulse-Width-Modulated (PWM) amplifier that translates the incoming signals into PWM commands and drives the motor. The rod is manually erected and stabilized before every trial.

FIGURE 8. QNET 2.0 rotary pendulum board.

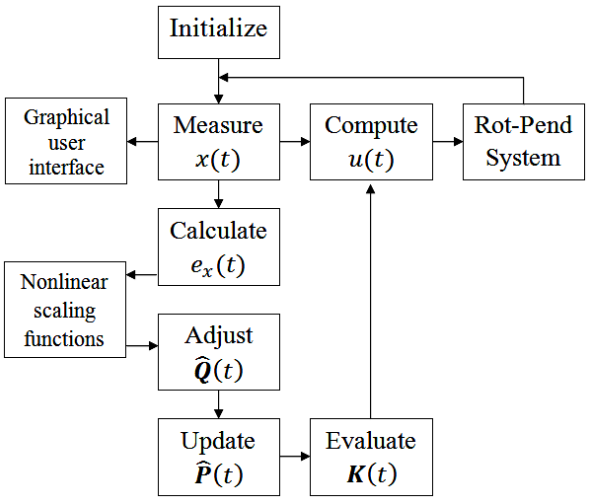

FIGURE 9. Flow-chart of control algorithm.

B. EXPERIMENTAL EVALUATION

The position-regulation and disturbance-rejection behavior of the proposed SM-STR is compared with the Baseline-STR and the standard fixed-gain LQR via "five" distinct hardware experiments. The details of these test-cases and the corresponding results yielded by each of the three aforementioned controllers are presented as follows.

1) POSITION REGULATION

The position-regulation behavior of the Rot-Pend system is analyzed by allowing its rod and arm to track their reference positions under normal conditions. The resulting time-domain profiles of θ, α, V_m, and $\boldsymbol{K}(t)$ are shown in Figure 10.

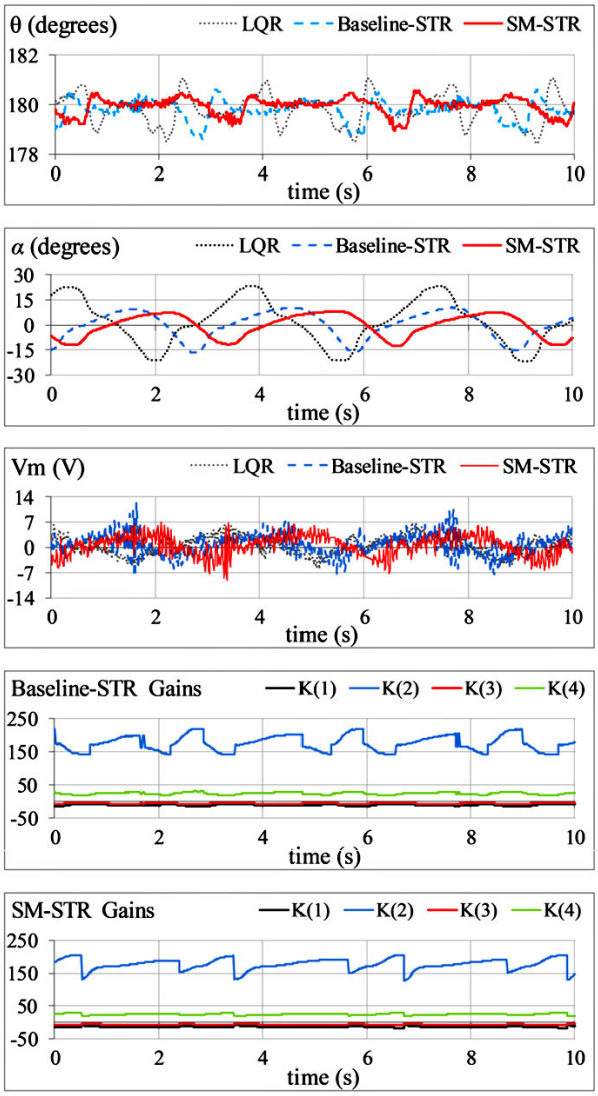

FIGURE 10. Pendulum's response under normal conditions.

2) IMPULSIVE-DISTURBANCE COMPENSATION

The controller's immunity against bounded disturbances is examined by injecting a pulse signal, having a magnitude of $+5.0$ V and duration of 100.0 ms, in the control input signal. The disturbance signal is applied at the time-instants when the arm-angle's response approaches its second and third maxima. The variations in the response of θ, α, V_m, and $\boldsymbol{K}(t)$, rendered by each controller, are shown in Figure 11.

3) STEP-DISTURBANCE COMPENSATION

The controller's ability to reject the detrimental effect of abrupt parametric variations and permanent load changes is assessed by applying a $+5.0$ V step-signal in the control input at $t \approx 4.0$ s mark. The resulting variations in the time-domain profiles of θ, α, V_m, and $\boldsymbol{K}(t)$, rendered by each of the three control schemes, are shown in Figure 12.

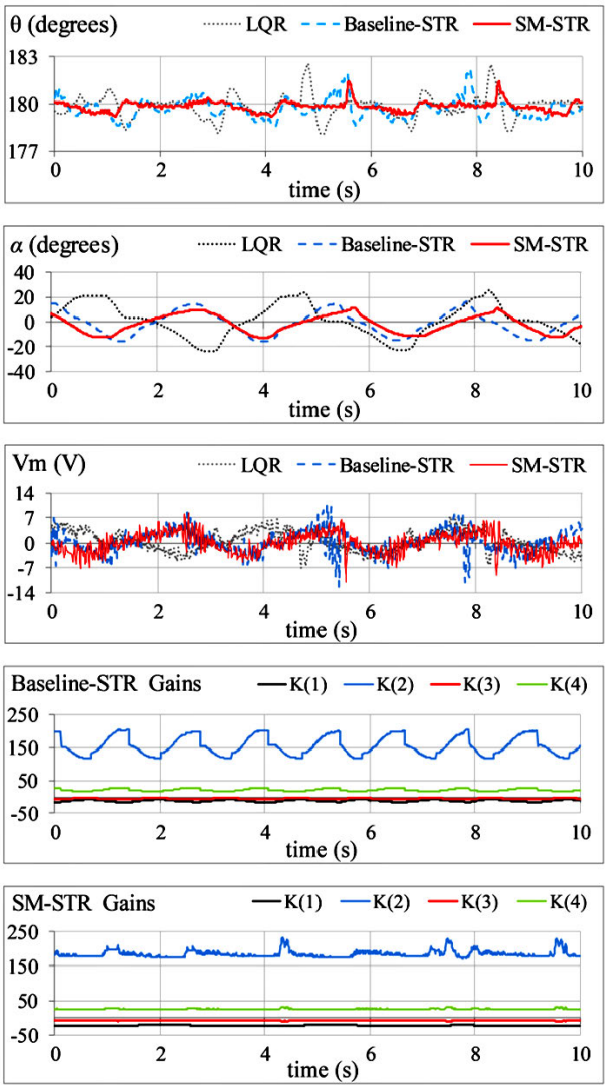

FIGURE 11. Pendulum's response under impulsive disturbances.

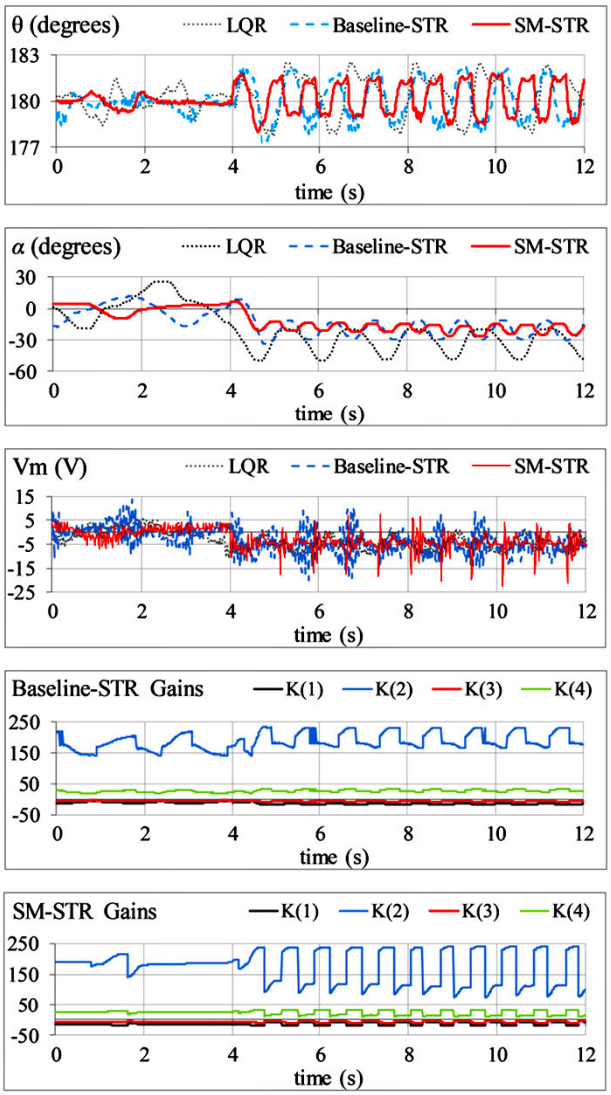

FIGURE 12. Pendulum's response under step disturbance.

4) NOISE IMMUNITY

The controller's ability to mitigate the effects of process noise contributed by the mechanical vibrations or electronic components is assessed by injecting a low-amplitude and high-frequency sinusoidal signal, $d(t) = 1.5\sin(20\pi t)$, in the reference input at $t \approx 0$ s. The corresponding time-domain responses associated with θ, α, V_m, and $\boldsymbol{K}(t)$ are shown in Figure 13.

5) MODELING-ERROR ATTENUATION

The controller's robustness against the modeling and identification errors is tested by permanently modifying the state-space model of the system. This is done by attaching a 0.10 kg mass beneath the base of pendulum's rotating arm via a hook, as shown in Figure 14. The proposed modification is introduced in the system at $t \approx 4.0$ s mark. The resulting time-domain profiles of θ, α, V_m, and $\boldsymbol{K}(t)$ are shown in Figure 15.

C. ANALYSIS AND DISCUSSIONS

The experimental results of each test case are comparatively analyzed in terms of the following Key-Performance-Indicators (KPIs):

- The time taken (t_s) by the "rod" to settle within ± 0.1 deg. of reference after recovering from a transient.
- The magnitude of peak overshoot or undershoot (M_p) in the rod's angular response.
- The root-mean-square-error ($RMSE_x$) in the responses of α and θ.
- The offset-error (OE_α) in the arm-angle under step-disturbance, the peak-to-peak amplitude of oscillations (x_{p-p}) in the response under disturbances.
- The mean-square-voltage input (P_v) applied to the DC motor to stabilize the pendulum.
- The magnitude of peak voltage spike (M_v) recorded in the control-input profile under disturbances.

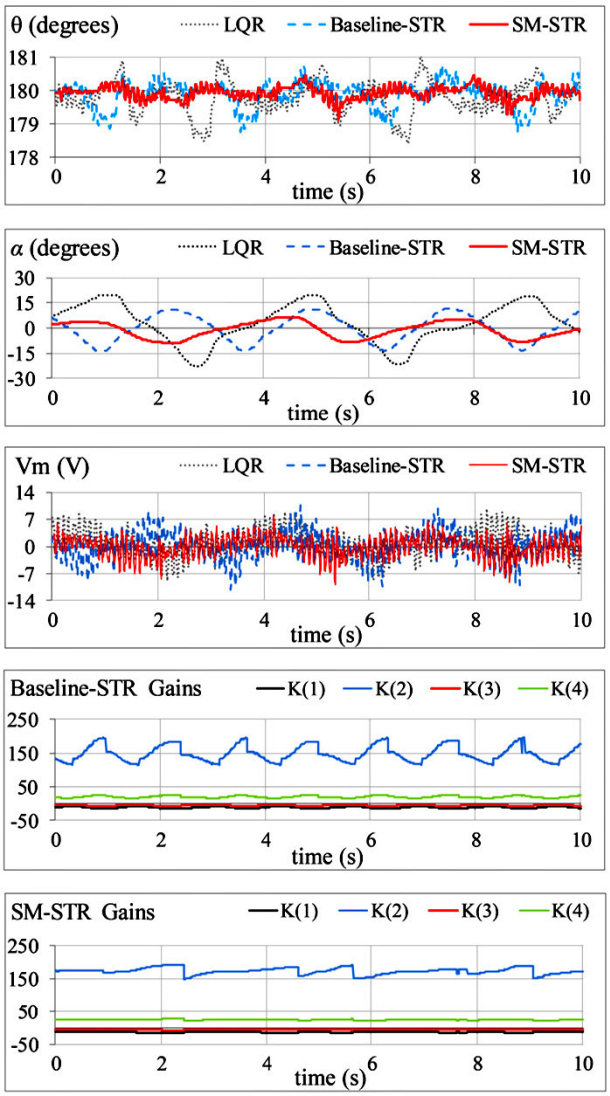

FIGURE 13. Pendulum's response under sinusoidal disturbance.

FIGURE 14. Pendulum setup with 0.10 kg mass attached to arm.

TABLE 5. Summary of experimental results.

Test	KPI	Controllers		
		LQR	Baseline-STR	SM-STR
A	$RMSE_\theta$ (deg.)	0.64	0.45	0.35
	$RMSE_\alpha$ (deg.)	13.77	8.07	6.88
	P_v (V^2)	6.39	8.83	7.80
B	$RMSE_\theta$ (deg.)	0.75	0.67	0.35
	$\lvert M_{p,\theta}\rvert$ (deg.)	2.61	2.20	1.42
	t_s (s)	0.94	0.70	0.42
	$RMSE_\alpha$ (deg.)	13.45	9.46	7.35
	$\lvert M_v\rvert$ (V)	7.30	12.33	10.91
	P_v (V^2)	8.10	9.13	7.75
C	$RMSE_\theta$ (deg.)	1.25	1.15	0.98
	$\theta_{p\text{-}p}$ (deg.)	4.30	3.74	2.91
	$RMSE_\alpha$ (deg.)	28.80	18.10	16.57
	$\alpha_{p\text{-}p}$ (deg.)	29.25	17.08	8.77
	OE_α (deg.)	-33.15	-20.08	-17.86
	$\lvert M_v\rvert$ (V)	10.73	21.27	22.52
	P_v (V^2)	26.05	37.85	24.78
D	$RMSE_\theta$ (deg.)	0.54	0.41	0.20
	$RMSE_\alpha$ (deg.)	12.17	7.94	4.96
	P_v (V^2)	12.40	13.22	7.85
E	$RMSE_\theta$ (deg.)	1.02	0.86	0.54
	$\theta_{p\text{-}p}$ (deg.)	4.38	3.35	2.58
	$RMSE_\alpha$ (deg.)	17.42	11.45	9.64
	P_v (V^2)	10.86	16.83	12.24

The numerical values of these KPIs are recorded in Table 5. A concise assessment of the experimental results is presented as follows. In Test-A, the SM-STR demonstrates minimum reference tracking error as compared to other controllers. The rod remains well within ± 1.0 deg. of the reference with minimal oscillations. It exhibits relatively smaller peaks in the control input profile as compared to the Baseline-STR. In Test-B, the SM-STR manifests the most time-optimal behavior. It effectively rejects the impulsive disturbances by attenuating the peaks in the response and successfully mitigates the succeeding oscillations, while exhibiting minimum-time transient recovery. Moreover, the overall control energy expenditure and the peak servo requirements of SM-STR are considerably lesser than the Baseline-STR. In Test-C, the step-disturbance permanently displaces the arm from its reference position. However, the SM-STR demonstrates strong damping against this disturbance by exhibiting minimum offset-error in α. It effectively minimizes the peak-to-peak amplitude of oscillations in the angular responses of α and θ that are contributed by the disturbance. Moreover, the SM-STR consumes significantly lesser control energy than the Baseline-STR. In Test-D, the SM-STR shows the best position-regulation behavior. It suppresses the oscillations in the response and also significantly reduces the control input consumption. Despite the noise, the system manages to regulate the arm and the rod at the corresponding reference positions with minimal RMSE.

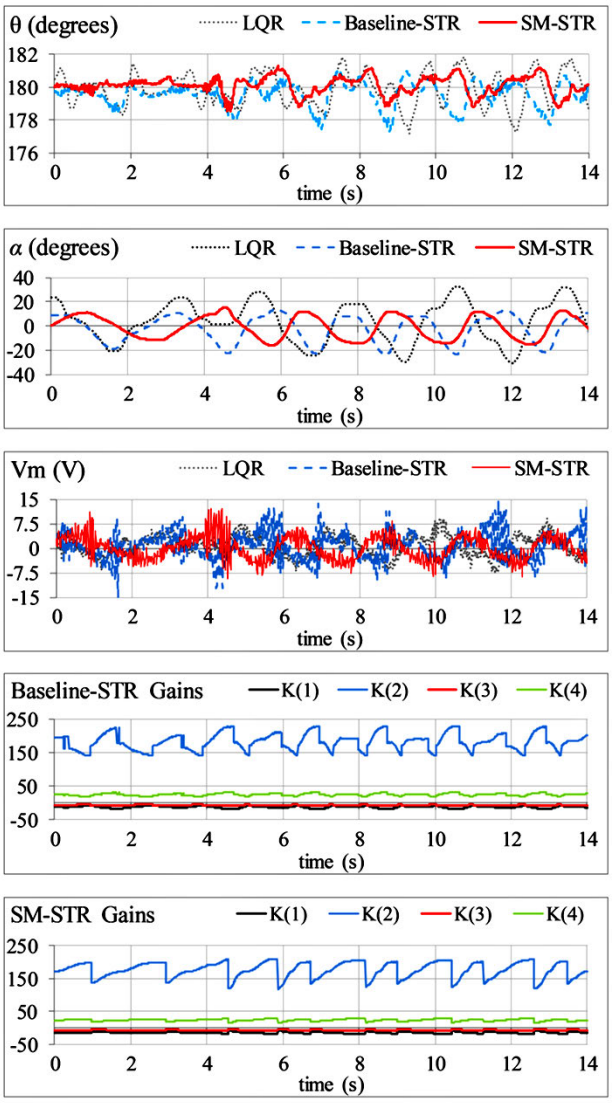

FIGURE 15. Pendulum's response under modeling error.

In Test-E, the LQR exhibits large oscillations in the response while balancing the rod. The SM-STR quickly compensates the modeling error and offers strong damping to mitigate the peak-to-peak amplitude of oscillations.

The experimental analysis clearly validates the superior robustness of the SM-STR in every test-case. The fixed-gain LQR exhibits the poorest position-regulation behavior while consuming lesser control-input energy as compared to the Baseline-STR. The Baseline-STR shows reasonable improvement in disturbance-rejection capability as compared to standard LQR, at the cost of high control energy consumption. The SM-STR manifests minimum transition times, minimum magnitude of overshoots, minimum reference-tracking error, and economical control input expenditure. It consumes relatively larger control input energy than the LQR (in Tests A and E, only). However, its consumption is much lesser than that of Baseline-STR in every scenario. The proposed adaptive scheme safeguards the controller's stability under every operating condition.

VII. CONCLUSION

The novel contribution of this paper is to devise a stable and indirect self-tuning control framework for under-actuated multivariable systems in order to enhance their disturbance-rejection capability against environmental indeterminacies by rendering rapid transits, superior attenuation against fluctuations, and reasonable control input economy in the response. This objective is achieved by augmenting the controller's quadratic cost-function with state-error driven continuous nonlinear scaling functions that adaptively modulate the state weighting-coefficients. This paper contributes to systematically formulate an original self-mutating adaptation mechanism that employs pre-calibrated SHFs to attune the weighting-coefficients. The self-mutating SHFs autonomously change their structure under different phases of the response by using well-postulated pre-defined logical rules. This augmentation obviates the necessity of empirically tuning the weighting-coefficients, enhances the adaptability of controller, and enables it to efficiently mitigate the detrimental effects of parametric uncertainties. The proposed adaptive tuning system is computationally economical as it does not put iterative computational burden on the embedded processor. Credible hardware experiments are conducted on the QNET 2.0 Rot-Pend system to validate the superior disturbance-rejection capability of SM-STR. Its enhanced robustness is accredited to the increased degrees-of-freedom offered by the self-mutating SHFs augmented with auxiliary DM modules, which enables the system to quickly respond to the parametric variations and modify the controller's behavior accordingly. In future, soft-computing techniques can be employed to efficiently alter the weighting-coefficients online. Moreover, the proposed adaptive controller can be applied to regulate the closed-loop performance of other electro-mechanical systems in order to further investigate its controlling capabilities.

REFERENCES

[1] M. Szuster and Z. Hendzel, "Control of mechatronic systems," in *Intelligent Optimal Adaptive Control for Mechatronic Systems*, Berlin, Germany: Springer, 2017, ch. 7, pp. 127–254.
[2] S. Bicakci, "On the implementation of fuzzy VMC for an under actuated system," *IEEE Access*, vol. 7, pp. 163578–163588, 2019.
[3] W. Guo and D. Liu, "Sliding mode observe and control for the underactuated inertia wheel pendulum system," *IEEE Access*, vol. 7, pp. 86394–86402, 2019.
[4] T. Yang and Y. Li, "Finite-time control for a class of inverted pendulum systems," *IEEE Access*, vol. 7, pp. 129637–129643, 2019.
[5] Z. Li, C. Yang, and L. L. Fan, "Linear Control," in *Advanced Control of Wheeled Inverted Pendulum Systems*, London, U.K.: Springer, 2013, ch. 4, pp. 55–76.
[6] O. S. Bhatti, K. Mehmood-Ul-Hasan, and M. A. Imtiaz, "Attitude control and stabilization of a two-wheeled self-balancing robot," *Control Eng. Appl. Inform.*, vol. 17, no. 3, pp. 98–104, 2015.
[7] H. O. Erkol, "Optimal PI$^{\lambda}$D$^{\mu}$ controller design for two wheeled inverted pendulum," *IEEE Access*, vol. 6, pp. 75709–75717, 2018.

[8] I. K. Ibraheem and G. A. Ibraheem, "Motion control of an autonomous mobile robot using modified particle swarm optimization based fractional order PID controller," *J. Eng. Technol.*, vol. 34, no. 13, pp. 2406–2419, 2016.
[9] E. Susanto, A. S. Wibowo, and E. G. Rachman, "Fuzzy swing up control and optimal state feedback stabilization for self-erecting inverted pendulum," *IEEE Access*, vol. 8, pp. 6496–6504, 2020.
[10] I. Shah and F. U. Rehman, "Smooth second order sliding mode control of a class of underactuated mechanical systems," *IEEE Access*, vol. 6, pp. 7759–7771, 2018.
[11] A. J. Humaidi, A. H. Hameed, and I. K. Ibraheem, "Design and performance study of two sliding mode backstepping control schemes for roll channel of delta wing aircraft," in *Proc. 6th Int. Conf. Control, Decis. Inf. Technol. (CoDIT)*, Paris, France, Apr. 2019, pp. 1215–1220.
[12] O. Saleem, M. Rizwan, and M. Ahmad, "Augmented linear quadratic tracker for enhanced output-voltage control of DC-DC buck converter," *Control Eng. Appl. Inform.*, vol. 20, no. 4, pp. 40–49, 2018.
[13] L. B. Prasad, B. Tyagi, and H. O. Gupta, "Optimal control of nonlinear inverted pendulum system using PID controller and LQR: Performance analysis without and with disturbance input," *Int. J. Autom. Comput.*, vol. 11, no. 6, pp. 661–670, Dec. 2014.
[14] O. Saleem and K. Mahmood-Ul-Hasan, "Robust stabilisation of rotary inverted pendulum using intelligently optimised nonlinear self-adaptive dual fractional-order PD controllers," *Int. J. Syst. Sci.*, vol. 50, no. 7, pp. 1399–1414, May 2019.
[15] O. S. Bhatti, O. B. Tariq, A. Manzar, and O. A. Khan, "Adaptive intelligent cascade control of a ball-riding robot for optimal balancing and station-keeping," *Adv. Robot.*, vol. 32, no. 2, pp. 63–76, Jan. 2018.
[16] S.-P. Li, "Adaptive control with optimal tracking performance," *Int. J. Syst. Sci.*, vol. 49, no. 3, pp. 496–510, Feb. 2018.
[17] B. Gruenwald and T. Yucelen, "On transient performance improvement of adaptive control architectures," *Int. J. Control*, vol. 88, no. 11, pp. 2305–2315, Nov. 2015.
[18] O. Saleem, M. Rizwan, K. Mahmood-Ul-Hasan, and M. Ahmad, "Performance enhancement of multivariable model reference optimal adaptive motor speed controller using error-dependent hyperbolic gain functions," *Automatika*, vol. 61, no. 1, pp. 117–131, Jan. 2020.
[19] R. Ganapathy Subramanian and V. K. Elumalai, "Robust MRAC augmented baseline LQR for tracking control of 2 DoF helicopter," *Robot. Auto. Syst.*, vol. 86, pp. 70–77, Dec. 2016.
[20] M. Waszak and R. Langowski, "An automatic self-tuning control system design for an inverted pendulum," *IEEE Access*, vol. 8, pp. 26726–26738, 2020.
[21] Z. Song, J. Liu, Y. Hu, Y. Cheng, and F. Tan, "Real-time performance analyses and optimal gain-scheduling control of offshore wind turbine under ice creep loads," *IEEE Access*, vol. 7, pp. 181706–181720, 2019.
[22] Y. Bolea, V. Puig, and J. Blesa, "Gain-scheduled smith predictor PID-based LPV controller for open-flow canal control," *IEEE Trans. Control Syst. Technol.*, vol. 22, no. 2, pp. 468–477, Mar. 2014.
[23] F. D. Bianchi, C. Kunusch, C. Ocampo-Martinez, and R. S. Sanchez-Pena, "A gain-scheduled LPV control for oxygen stoichiometry regulation in PEM fuel cell systems," *IEEE Trans. Control Syst. Technol.*, vol. 22, no. 5, pp. 1837–1844, Sep. 2014.
[24] L. Guarnaccia, R. Bevilacqua, and S. P. Pastorelli, "Suboptimal LQR-based spacecraft full motion control: Theory and experimentation," *Acta Astronautica*, vol. 122, pp. 114–136, May 2016.
[25] H. Zhang, J. Wang, and G. Lu, "Self-organizing fuzzy optimal control for under-actuated systems," *J. Syst. Control Eng.*, vol. 228, no. 8, pp. 578–590, 2014.
[26] Z. Ma, Y. Fang, H. Zheng, and L. Liu, "Active disturbance rejection control with self-adjusting parameters for vibration displacement system of continuous casting mold," *IEEE Access*, vol. 7, pp. 52498–52507, 2019.
[27] W. Riyadh and I. Kasim, "From PID to nonlinear state error feedback controller," *Int. J. Adv. Comput. Sci. Appl.*, vol. 8, no. 1, pp. 312–322, 2017.
[28] A. J. Humaidi and I. K. Ibraheem, "Speed control of permanent magnet DC motor with friction and measurement noise using novel nonlinear extended state observer-based anti-disturbance control," *Energies*, vol. 12, no. 9, p. 1651, 2019.
[29] A. A. Najm and I. K. Ibraheem, "Altitude and attitude stabilization of UAV quadrotor system using improved active disturbance rejection control," *Arabian J. Sci. Eng.*, vol. 45, no. 3, pp. 1985–1999, Mar. 2020.
[30] O. Saleem and K. Mahmood-Ul-Hasan, "Adaptive collaborative speed control of PMDC motor using hyperbolic secant functions and particle swarm optimization," *Turkish J. Electr. Eng. Comput. Sci.*, vol. 26, no. 3, pp. 1612–1622, 2018.
[31] B. Armstrong and B. A. Wade, "Nonlinear PID control with partial state knowledge: Damping without derivatives," *Int. J. Robot. Res.*, vol. 19, no. 8, pp. 715–731, Aug. 2000.
[32] O. Saleem and U. Omer, "EKF-based self-regulation of an adaptive nonlinear PI speed controller for a DC motor," *Turkish J. Electr. Eng. Comput. Sci.*, vol. 25, pp. 4131–4141, Oct. 2017.
[33] B. M. Isayed and M. A. Hawwa, "A nonlinear PID control scheme for hard disk drive servosystems," in *Proc. IEEE-MED*, Athens, Greece, Jun. 2007, pp. 1–6.
[34] J. Huang, T. Zhang, Y. Fan, and J.-Q. Sun, "Control of rotary inverted pendulum using model-free backstepping technique," *IEEE Access*, vol. 7, pp. 96965–96973, 2019.
[35] O. Saleem, U. T. Shami, K. Mahmood-Ul-Hasan, F. Abbas, and S. Mahmood, "Robust-optimal output-voltage control of buck converter using fuzzy adaptive weighted combination of linear feedback controllers," *Control Eng. Appl. Inform.*, vol. 21, no. 2, pp. 43–53, 2019.
[36] F. L. Lewis, D. Vrabie, and V. L. Syrmos, "Optimal control of continuous-time systems," in *Optimal Control*, 3rd ed. Hoboken, NJ, USA: Wiley, 2012, ch. 3, pp. 110–167.
[37] O. Saleem and U. Omer, "Synergistic speed control strategy for PMDC motor," in *Proc. Int. Multi-topic Conf. (INMIC)*, Lahore, Pakistan, Nov. 2017, pp. 1–6.
[38] V. M. Hernandez-Guzman, M. Antonio-Cruz, and R. Silva-Ortigoza, "Linear state feedback regulation of a Furuta pendulum: Design based on differential flatness and root locus," *IEEE Access*, vol. 4, pp. 8721–8736, 2016.
[39] N. Farah, M. H. N. Talib, N. S. M. Shah, Q. Abdullah, Z. Ibrahim, J. B. M. Lazi, and A. Jidin, "A novel self-tuning fuzzy logic controller based induction motor drive system: An experimental approach," *IEEE Access*, vol. 7, pp. 68172–68184, 2019.

OMER SALEEM received the bachelor's and master's degrees in electrical engineering with specialization in control systems from the University of Engineering and Technology (U.E.T.), Lahore, Pakistan, where he is currently pursuing the Ph.D. degree with specialization in adaptive control systems. He is currently serving as an Assistant Professor with the Department of Electrical Engineering, National University of Computer and Emerging Sciences, Lahore. He has published several research articles in high-indexed journals. His research interests include the design of adaptive and self-tuning state-feedback control systems for mechatronic systems and power electronic converters using nonlinear sliding surfaces and expert systems.

KHALID MAHMOOD-UL-HASAN received the Ph.D. degree in electrical engineering with specialization in control systems from the University of Bradford, U.K. He is currently serving as a Professor and the Chairman of the Department of Electrical Engineering, University of Engineering and Technology, Lahore, Pakistan. His research interests include linear systems theory, digital control systems, and the control of electrical machine drives.